Available online at www.sciencedirect.com
SCIENCE DIRECT
ELSEVIER
Polymer 46 (2005) 9348–9361
polymer
www.elsevier.com/locate/polymer

Synthesis, thermal properties, and specific interactions of high T_g increase in poly(2,6-dimethyl-1,4-phenylene oxide)-*block*-polystyrene copolymers

Shiao-Wei Kuo[a,*], Chih-Feng Huang[a], Pao-Hsiang Tung[a], Wu-Jiang Huang[b], Jien-Ming Huang[c], Feng-Chih Chang[a]

[a]*Institute of Applied Chemistry, National Chiao Tung University, Hsin Chu, Taiwan, ROC*
[b]*Department of Environmental Science and Engineering, National Ping-Tung University of Science and Technology, Ping-Tun, Taiwan, ROC*
[c]*Department of Chemical Engineering, Van Nung University, Chungli, Taiwan, ROC*

Received 20 May 2005; received in revised form 10 July 2005; accepted 14 July 2005
Available online 8 August 2005

Abstract

We have synthesized a series of block copolymers of poly(2,6-dimethyl-1,4-phenylene oxide) and polystyrene (PPO-*b*-PS copolymer) by atom transfer radical polymerization. The PS content in these copolymer systems was determined by using infrared spectroscopy, thermal gravimetric analysis, and solution and solid-state NMR spectroscopy; good correlations exist between these characterization methods. DSC analyses indicated that the PPO-*b*-PS copolymers have higher glass transition temperatures than do their corresponding PPO/PS blends. Our FTIR and solid-state NMR spectroscopic analyses suggest that the PPO-*b*-PS copolymers possess stronger specific interactions that are responsible for the observed relatively higher values of T_g. We found one single dynamic relaxation from the dynamic mechanical analysis, which implies dynamic homogeneity exists in the PPO-*b*-PS copolymer; this result is consistent with the one single proton spin–lattice relaxation time observed in the rotating frame [$T_{1\rho}$(H)] during solid state NMR spectroscopic analysis. In addition, the 2D FTIR spectroscopy reveals evidence for the stronger interactions between segments of PPO and PS through the formation of π-cation complexes.

Keywords: ATRP; Block copolymer; Specific interactions

1. Introduction

Miscible polymer blends provide a cost-effective method for developing new materials in polymer science industries by avoiding the need to develop new polymers. For example, the well known poly(2,6-dimethyl-1,4-phenylene oxide)/polystyrene (PPO/PS) miscible blend system has widespread commercial use in the thermoplastics industry [1–3]. The glass transition temperature (T_g) of a polymer is an important intrinsic characteristic that influences its material properties and potential applications. Furthermore, polymers having high values of T_g are attractive for industrial applications because of strong economic rewards. It is well known that the dependence of the value of T_g on the composition of miscible PPO/PS blends obeys the Fox rule. In a previous study [4], we found that the values of T_g of poly(vinylphenol)/poly(vinylpyrrolidone) (PVPh/PVP) blends are substantially higher than the values predicted by the Fox rule, and that this phenomenon is due to the presence of hydrogen bonding interactions. Furthermore, DSC, FTIR and solid state NMR spectroscopic analyses suggest that the values of T_g and the strength of hydrogen bonding of PVPh-*co*-PVP copolymers are both greater than those of their corresponding PVPh/PVP blends at the same mole fractions of PVPh [5,6]. Therefore, in an attempt to raise the value of T_g of the miscible PPO/PS blend, in this study we synthesized the PPO-*b*-PS copolymer.

The desire to control polymer properties through the synthesis of block copolymers and complex macromolecular architectures is a continuing theme throughout polymer chemistry [7,8]. Block copolymers are remarkable self-assembling systems that can assume a wide variety of morphologies, including lamellar, hexagonal-packed cylindrical, and body-centered cubic micellar structures, as a result of the presence of two immiscible polymer chains connected by covalent bonds and depending on the relative

* Corresponding author. Tel.: +886 3 5131512; fax: +886 3 5723764.
E-mail address: kuosw@mail.nctu.edu.tw (S.-W. Kuo).

0032-3861/$ - see front matter © 2005 Elsevier Ltd. All rights reserved.
doi:10.1016/j.polymer.2005.07.044

volume fractions of the blocks [9–12]. The block copolymers that have well defined structures, such as known molecular weights, molecular weight distributions, compositions, architectures, and end group functionalities, are in high demand. Such block copolymers have been synthesized in three ways [13]: (1) Sequential monomer addition, (2) coupling reactions of 'living' polymer chains, and (3) mechanism transformation. The development of ionic polymerization methods has allowed the preparation of copolymers with controlled chain-end functionalities and well-defined blocks and grafts [14–17]. These polymerizations, however, must be undertaken with nearly complete exclusion of moisture and often at very low temperatures. Moreover, only a few types monomers can be polymerized through these routes, and the use of more-functionalized monomers may cause undesired side reactions to occur. Recently, Matyjaszewski and Sawamoto [18] et al. have reported that atom transfer radical polymerization (ATRP) allows the synthesis of polymers that have narrow molecular weight distributions [19] and of well defined block copolymers [20,21] and star polymers [22,23]. ATRP has gained tremendous interest lately because it is tolerant of impurities, adventitious water, and high temperatures. The ATRP process uses an alkyl halide as initiator, a metal in its lower oxidation state, and complexing ligands [24–31]. The process involves the successive transfer of the halide from the dormant polymer chain to the ligated metal complex, thus establishing a dynamic equilibrium between the active and dormant species. This controlled radical polymerization allows the polymerization of a wide range of monomers, such as styrenes, acrylates, and methacrylates, as well as a variety of functional monomers.

In the literature, block copolymers having self-regular morphologies have emerged primarily from the investigation of diblock copolymers whose macrophase or microphase separation has been studied as a function of their compositions and interaction parameters. In contrast, we intended to synthesize PPO-*b*-PS block copolymers through ATRP, even though the PPO and PS units are well-known to form a miscible blend system [32–34]. Our approach was to modify the hydroxyl end group of PPO to form an α-haloester, which is one type of potential initiator for atom transfer radical polymerization.

FTIR and NMR spectroscopies are powerful tools for characterizing the detailed structures of polymers and their specific interactions because these features affect local electron densities so that corresponding frequency shifts can be observed [35–38]. Moreover, the phase behavior and molecular mobility of polymer blends or copolymers can be estimated from the proton spin–lattice relaxation time in the rotating frame $\left(T_{1\rho}^{\mathrm{H}}\right)$ measured by solid state NMR. The nature of the specific interactions in PPO/PS blends has been studied extensively. Based on solution NMR and X-ray photoelectron spectroscopic studies, Porter, Wang, and Goh have concluded that intermolecular interactions in PPO/PS blends exist between the methyl groups of PPO and the phenyl rings of PS [39–41]. In addition, proton spin diffusion experiments have indicated that PPO and PS units mix at a molecular level [42]. Recently, generalized two-dimensional (2D) correlation spectroscopy has been applied widely in polymer science [43]. This novel method can allow the specific interactions between polymer chains to be investigated by treating the spectral fluctuations as a function of time, temperature, pressure, and composition. Two-dimensional IR correlation spectroscopy can identify different intra- and intermolecular interactions through the analysis of selected bands from the 1D vibration spectrum. Noda [44] and Painter [45] have reported the 2D correlation IR spectra of PPO/PS blends. Noda's results suggest that the methyl groups of PPO segments in PPO/PS blends play an important role, but Painter's analysis of the same system concluded that the specific interaction between the PPO and PS chains probably is due to the formation of π-cation complexes [46,47] between the methyl groups of PPO and the aromatic rings of PS.

In this study, we have synthesized a series of block copolymers containing various PPO and PS contents to compare their glass transition temperatures with those of the corresponding PPO/PS blends. We have observed a significant glass transition temperature increase, relative to those of PPO/PS blends, by thermal analyses and have investigated the specific interactions present in these PPO-*b*-PS copolymers by using solid state NMR and 2D FTIR spectroscopies.

2. Experimental

2.1. Materials

Styrene was distilled from calcium hydride before use. Monomers were stored in a freezer. Copper (I) bromide (CuBr) was stirred in glacial acetic acid overnight, filtered, and then rinsed with absolute ethanol under a blanket of argon and dried under vacuum at 80 °C for 3 days. Toluene, THF, pyridine, and acetonitrile were distilled prior to use. *N*,*N*′,*N*″,*N*‴-pentamethyldiethylenetriamine (PMDETA) was used as received. PPO was purchased from GE Company (BLENDEX® HPP857).

2.2. Preparation of PPO/PS blends

Desired composition of PPO (BLENDEX® HPP857) and commercial PS (M_n = 45,000 g/mole, T_g = 100 °C) was dissolved in toluene at a concentration of 5 wt% and stirred for 6–8 h. These solutions were allowed to evaporate slowly at 50 °C for 1 day on a teflon plate and dried at 90 °C for 1 day to ensure total elimination of the solvent, and then further dried under vacuum at 90 °C for 2 days.

2.3. Preparation of the PPO-Br macroinitiator by the esterification of PPO

4-(Dimethylamino)pyridine (DMAP, 20 mg) was added to a stirred suspension of PPO (1.18 g, 5.9 mmol) in pyridine (1.9 mL, 23.6 mmol) and toluene (12 mL). 2-Bromopropionyl bromide (4.12 mL, 47.2 mmol) was then added dropwise over 1 h at 0 °C. The ice bath was removed and stirring was continued at 50 °C for 5 h. The mixture was then precipitated into 10-fold 5% H_2O/methanol to purify. The small peaks present at 180 ppm and 1750 cm^{-1} in the ^{13}C solution NMR and FTIR spectra, which correspond to the carbonyl group of the 2-bromopropionyl bromide unit, indicate that the PPO-Br macroinitiator has been synthesized successfully.

2.4. Preparation of PPO-b-PS by the ATRP of styrene with PPO-Br macroinitiator

A typical polymerization was carried out as follows: CuBr (0.4 mmol) was placed in a dry 25-mL round-bottom flask equipped with a stirrer bar. Degassed toluene (10 mL), monomer (40 mmol), and ligand (0.4 mmol) were added sequentially and the solution was stirred for 20 min to form the Cu complex. The initiator (0.1 mmol) was then added. The whole process was performed within a nitrogen-filled dry box. An aliquot of the solution (ca. 0.1 mL) was removed and then the bulk polymerization proceeded at an appropriate temperature in an oil bath. The reaction mixture turned dark green immediately and became progressively more viscous. Periodically, aliquots (0.1 mL) were removed for analysis. Typically, exotherms of 2–4 °C were observed, indicating that polymerization was occurring. Upon completion of the reaction, the mixture was diluted five-fold with tetrahydrofuran (THF) and stirred with Amberlite IR-120 (H form) cation-exchange resin (3–5 g) for 30–60 min to remove the catalyst. The mixture was then passed through an alumina column and precipitated into 10% H_2O/methanol (500 mL). This purification protocol resulted in the loss of up to ca. 5% of the polymer as a result of adsorption. The resulting polymers were filtered and dried overnight at 60 °C under vacuum. The chemistry and structures are summarized as follows:

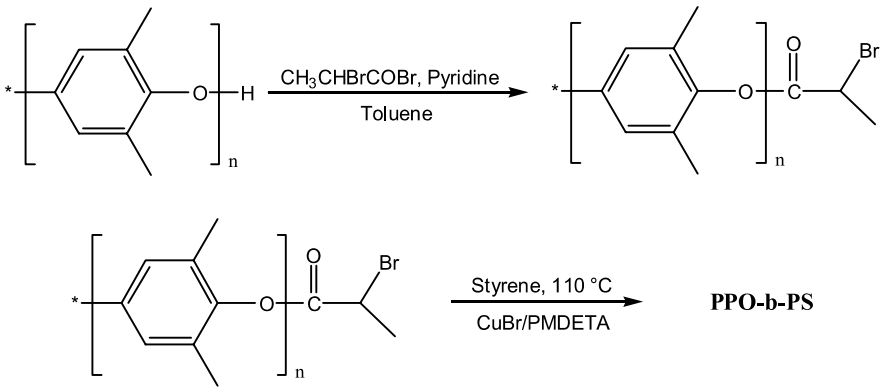

2.5. Gel permeation chromatography (GPC)

Molecular weights and molecular weight distributions were determined by gel permeation chromatography (GPC) using a Waters 510 HPLC—equipped with a 410 Differential Refractometer, a UV detector, and three Ultrastyragel columns (100, 500, and 10^3 Å) connected in series in order of increasing pore size—using THF as an eluent at a flow rate of 0.4 mL/min. The molecular weight calibration curve was obtained using polystyrene standards.

2.6. Solution NMR spectroscopy

^{13}C NMR spectra were recorded in $CDCl_3$ at 125 MHz on a Bruker AM 500 Spectrometer with the signal of the solvent's carbon atom serving as the internal standard.

2.7. Differential scanning calorimetry (DSC)

The glass transition temperature of the blend was measured using a DuPont DSC-9000 instrument at a scan rate of 20 °C/min over a temperature range from 30 to 260 °C. The sample (ca. 5–10 mg) was weighed and sealed in an aluminum pan. The sample was cooled rapidly to room temperature from the first scan and then up to 250 °C at a scan rate of 20 °C/min under a nitrogen atmosphere. The glass transition temperature is taken as the midpoint of the heat capacity transition between the upper and lower points of deviation from the extrapolated glass and liquid lines.

2.8. Thermal gravimetric analysis (TGA)

Thermal gravimetric analyses were conducted on a DuPont TGA 2950 instrument under an atmosphere of flowing nitrogen gas at a heating rate of 20 °C/min over a temperature range from 30 to 800 °C.

2.9. Dynamic mechanical analysis (DMA)

Dynamic mechanical analyses were performed using a TA Instruments DMA Q800 (DuPont) in a tension mode over a temperature range from 30 to 250 °C. Data

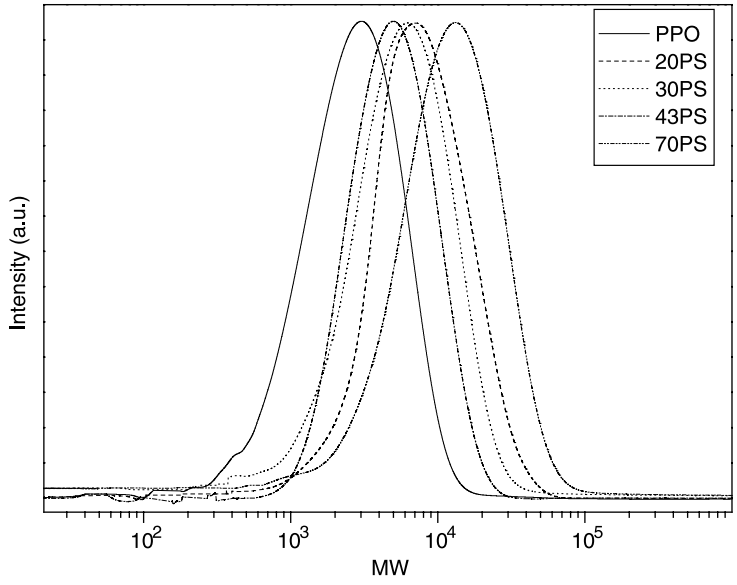

Fig. 1. GPC traces of PPO-*b*-PS copolymers having various PS contents.

acquisition and analyses of the storage modulus (E'), loss modulus (E''), and loss tangent ($\tan\delta$) were recorded automatically by the system. The heating rate and frequency were fixed at 2 °C/min and 1 Hz, respectively. Samples for DMA experiments were prepared by compression molding; the sample's dimensions were $4\times0.8\times0.2\ \text{cm}^3$.

2.10. Solid state NMR spectroscopy

High-resolution solid state ^{13}C NMR spectroscopy experiments were performed at room temperature using a Bruker DSX-400 spectrometer operating at resonance frequencies of 399.53 and 100.47 MHz for ^{1}H and ^{13}C nuclei, respectively. The ^{13}C CP/MAS spectra were measured with a 3.9-μs 90° pulse, a 3-s pulse delay time, a 30-ms acquisition time and 2048 scans were collected. All NMR spectra were recorded at 300 K using broad-band proton decoupling and a normal cross-polarization pulse sequence. A magic-angle sample-spinning (MAS) rate of 5.4 kHz was used to avoid absorption overlapping. The proton spin–lattice relaxation time in the rotating frame $\left(T_{1\rho}^{\text{H}}\right)$ was determined indirectly via carbon observation using a $90°-\tau$-spin lock pulse sequence prior to cross polarization. The data acquisition was performed through ^{1}H decoupling and delay times (τ) ranging from 0.1 to 12 ms with a contact time of 1.0 ms.

2.11. FTIR spectroscopy

FTIR spectra were obtained from a NaCl disk using a Nicolet Avatar 320 FTIR spectrometer, with 32 scans collected at a resolution of $1\ \text{cm}^{-1}$. A THF solution containing the sample was cast onto an NaCl disk and dried under conditions similar to those used in the bulk preparations. The sample chamber was purged with nitrogen to maintain the film's dryness. Two-dimensional correlation analysis was performed using 'Vertor 3D' software supplied by Bruker Instrument Co. All the spectra applied to the 2D correlation analysis were normalized and classified into two sets: A and B. The spectra in set A are those of PPO-*b*-PS copolymers; A18 refers to the copolymer having a PS content of 18 wt%. The spectra in set B are those of PPO/PS blends; B50 refers to the sample of PPO/PS = 50/50. Negative intensities of auto peaks or cross peaks in 2D

Table 1
The PPO-*b*-PS copolymer used in this study

Copolymer	Conditions $[M]_0/[I]_0/[CuBr]_0/[PMDETA]_0$	Yield (%)	M_n	PDI	T_g
Pure PPO	–	–	3200	2.10	163
20PS	100/1/1/1	41.0	6800	1.76	156
30PS	100/1/1/1	50.0	7700	1.81	153
43PS	200/1/1/1	51.8	11,000	1.85	142
70PS	200/1/1/1	59.4	14,120	1.94	125

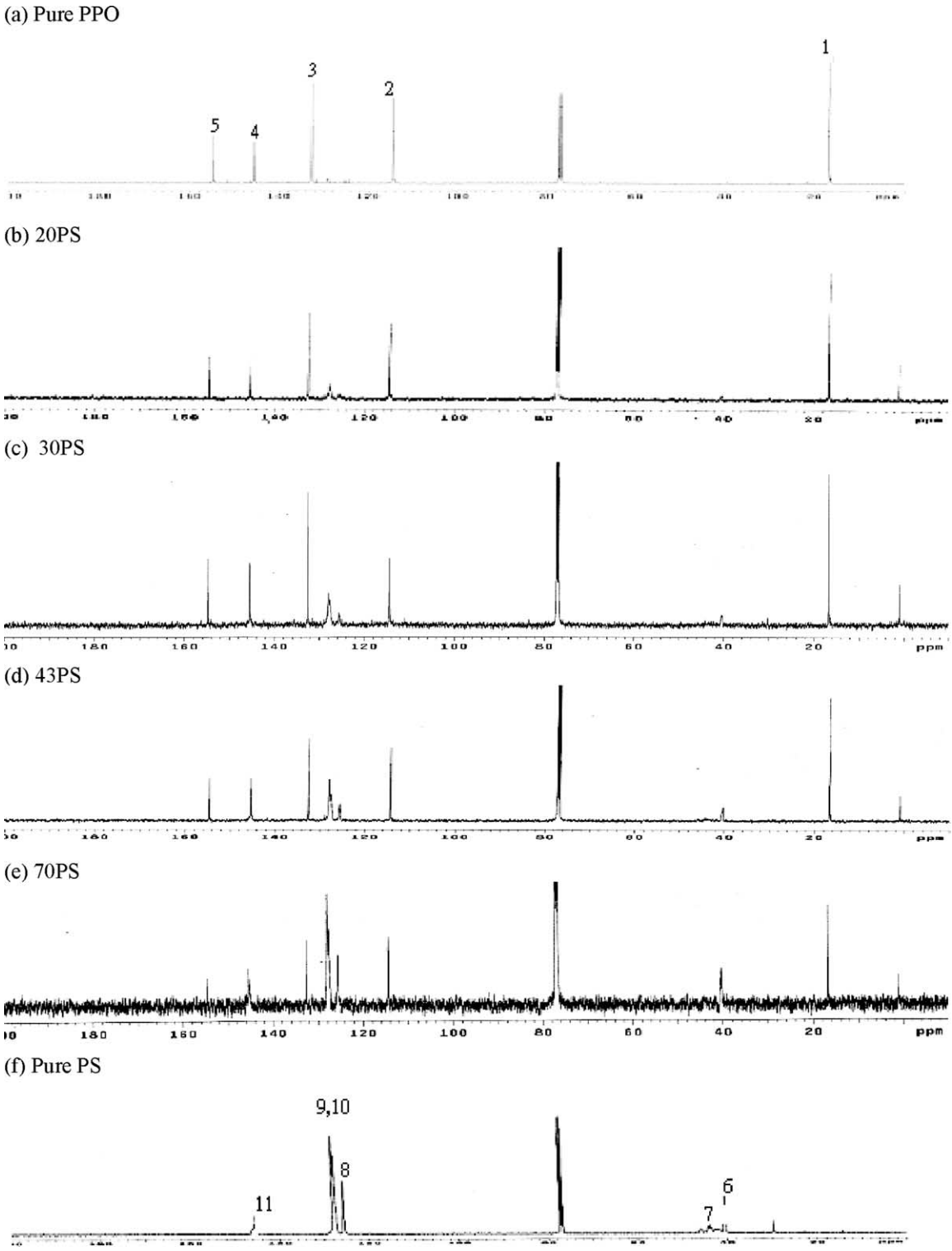

Fig. 2. Solution-phase ^{13}C NMR spectra of pure PPO, pure PS, and various PPO-*b*-PS copolymers.

correlation spectra are indicated by shaded regions; positive intensities are indicated by unshaded regions. Synchronous 2D spectra were used to study the specific interactions between PPO and PS in the blend; asynchronous 2D IR spectra were used to separate the bands of PPO from the spectra of PS in the blends or copolymers.

3. Results and discussion

3.1. Characterization of PPO-b-PS copolymers

GPC is a useful technique for determining the average molecular weights of polymers and it provides information

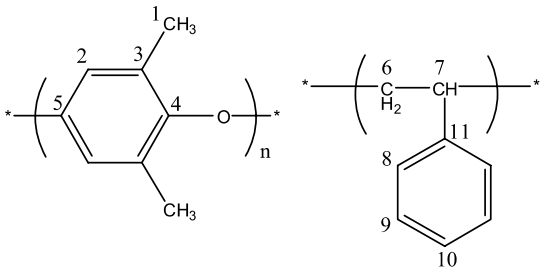

Scheme 1. Chemical structures of PPO and PS and their atom schemes in solution ^{13}C NMR.

on the structural integrity of the molecule. As shown in Fig. 1, block copolymers prepared from the PPO macroinitiator resulted in having high symmetry and monomodal GPC traces. The absence of the PPO macroinitiator peak supports the formation of PPO-*b*-PS block copolymers. Table 1 lists the average molecular weights and values of T_g determined for these synthesized PPO-*b*-PS copolymers. Various molecular weights of PPO-*b*-PS block copolymers were obtained, and for these block copolymers the polydispersity (PDI) did not exceed 2.1, which was originating from the PPO macroinitiator. Namely, block copolymerization of styrene gave relatively lower polydispersity due to the well-controlled procedure. The ^{13}C spectra of the pure PPO, pure PS, and various PPO-*b*-PS copolymers are presented in Fig. 2. The pure PPO and pure PS exhibit five and six signals (Scheme 1), respectively. The spectrum of the PPO-*b*-PS copolymer clearly displays peaks related to the resonance of pure PPO, a methylene group at 40 ppm, and aromatic carbon atoms at 128 ppm for pure PS. As a result, we confirm that the styrene monomer has indeed been incorporated into the PPO main chain. To determine the PS content in these PPO-*b*-PS copolymers, it is convenient to monitor the FTIR spectroscopic absorptions at 700 cm^{-1} (C–H out-of-plane bending vibration of the aromatic rings of PS) and 856 cm^{-1} (C–H bending of PPO). For convenience, we turn our attention on the infrared spectra of pure PPO, pure PS, and various PPO/PS blends measured at room temperature in the range from 650 to 900 cm^{-1} [Fig. 3(a)]. Clearly, the absorptions at 856 and 700 cm^{-1} can be assigned as the PPO and PS, respectively. For the PPO/PS blend system, we obtained a calibration curve of the intensity of PS at 700 cm^{-1} plotted against the weight percent of PS as shown in Fig. 4; using this curve, we can readily determine the composition of the PPO-*b*-PS copolymer, as indicated in Fig. 4(b). Fig. 5 displays the thermal gravimetric curves of pure PPO, pure PS, and various PPO-*b*-PS copolymers. Clearly, pure PPO is more thermally stable than is PS, and the TGA curves for the copolymers are situated between those of pure PPO and pure PS. The PS content of these copolymer systems also can be determined by their char yields relative to that of pure PPO. Table 2 summarizes the PS contents of these block copolymer systems determined by using infrared spectroscopy, thermal gravimetric analysis, and solution and solid state NMR spectroscopy; good correlations exists among these characterization methods.

3.2. Thermal properties of PPO-b-PS copolymers

Generally, it is believed that only a single glass transition temperature can be observed if the component polymers are thermodynamically miscible. Differential scanning calorimetry (DSC) is a convenient method for observing the thermal characteristics that arise from the different interactions of miscible copolymers and polymer blends. Fig. 6, which presents the DSC thermograms of various PPO/PS blends and PPO-*b*-PS copolymers having varying PS contents, reveals that all of the PPO/PS blends and PPO-*b*-PS copolymers have only a single glass transition temperature; this finding suggests strongly that these blends

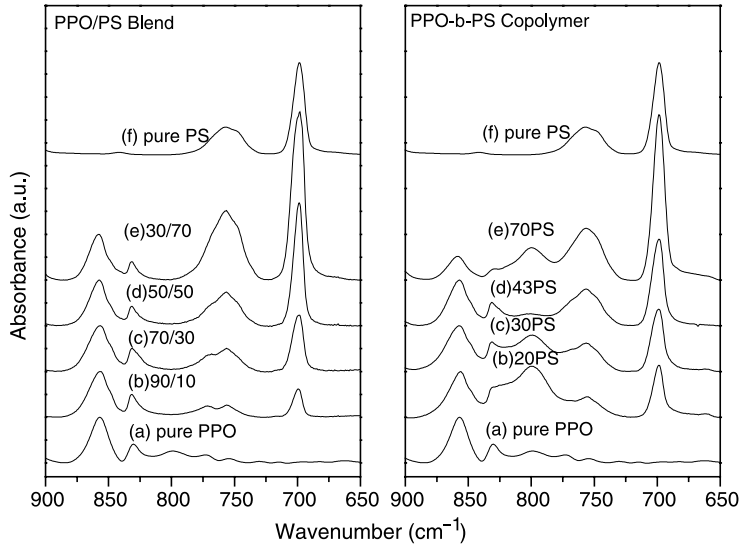

Fig. 3. FTIR spectra in the region 650–900 cm^{-1} for (a) PPO/PS blends and (b) PPO-*b*-PS copolymers.

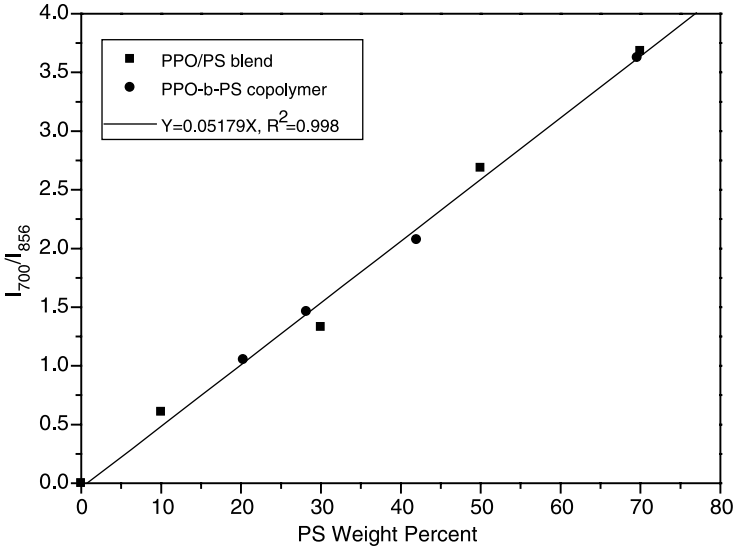

Fig. 4. Calibration curve for determining component contents of PS using the area ratios of absorption bands of PS at 700 cm^{-1}, and PPO at 856 cm^{-1}.

and copolymers are fully miscible and exist in a homogeneous amorphous phase. Meanwhile, the single values of T_g are observed between those of the mother polymers and the values of T_g in both the blend and copolymer systems increase upon increasing the PPO content, as is expected. Fig. 7 displays the glass transition temperatures and T_g breadths of PPO/PS blends and PPO-*b*-PS copolymers. Clearly, the values of T_g of PPO-*b*-PS copolymers are substantially and consistently higher than those of the PPO/PS blends over the entire range of compositions. It is worth noting that the dependence of the values of T_g on the composition of the PPO/PS blends is predicted by the Fox rule, while those of the PPO-*b*-PS copolymers are significantly higher than the predicted values. Fortunately, a more suitable equation, which is applicable to polymer blends or copolymers that feature specific interactions, is the Kwei equation [48]:

$$T_g = \frac{W_1 T_{g1} + kW_2 T_{g2}}{W_1 + kW_2} + qW_1 W_2 \quad (1)$$

where W_1 and W_2 are component weight fractions, T_{g1} and T_{g2} represent the corresponding glass transition temperatures, and k and q are fitting constants. We obtain the values $k=1$ and $q=30$ for the PPO-*b*-PS copolymers and $k=1$ and $q=-30$ for the PPO/PS blends. The parameter q corresponds to the strength of the specific interaction in a copolymer or polymer blend. Therefore, the difference in q that we observe between the two systems can be interpreted as indicating that the strength of the specific interactions within the PPO-*b*-PS copolymers is greater than that in the corresponding PPO/PS blend, which is consistent with the differences in the glass transition temperatures observed for the PPO-*b*-PS copolymer and the PPO/PS blend. It is worth

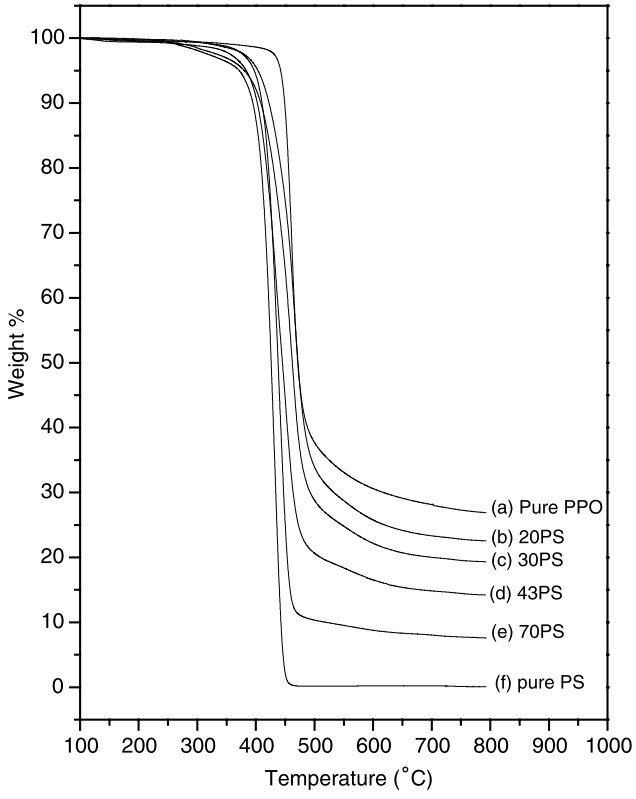

Fig. 5. TGA thermograms of pure PPO, pure PS, and PPO-*b*-PS copolymers having various PS contents.

Table 2
The PS content in the PPO-*b*-PS copolymers determined using various methods of characterization

Copolymer	^{13}C Solution NMR	^{13}C Solid-state NMR	FTIR	TGA
Pure PPO	–	–	–	–
20PS	15.4	22.0	20.3	17.9
30PS	31.7	32.8	31.0	29.6
43PS	45.5	47.0	42.6	48.0
70PS	74.8	78.0	70.0	72.2

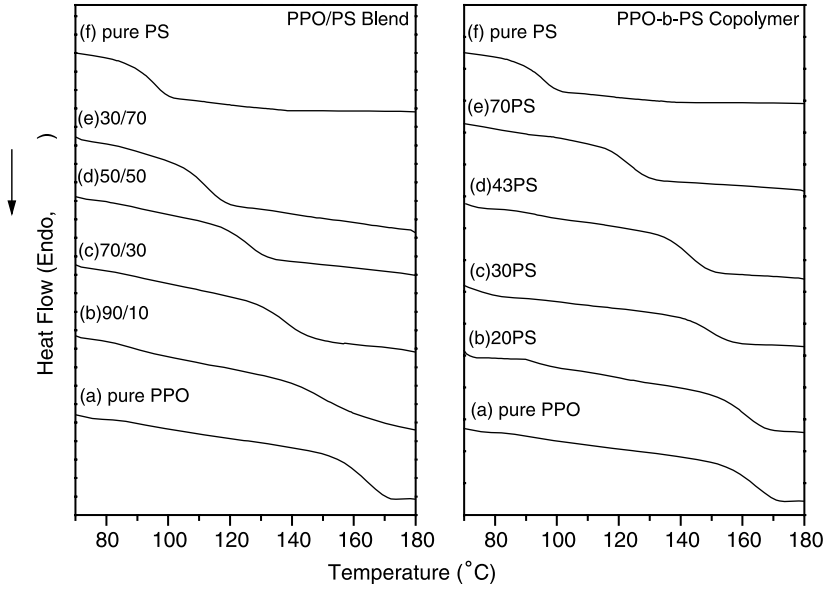

Fig. 6. DSC traces recorded from (a) PPO/PS blends and (b) PPO-*b*-PS copolymers.

noting that the value of T_g of the PPO-*b*-PS copolymer having a PS content of 70 wt% is about the same as that of the PPO/PS = 50/50 blend. Thus, at an identical value of T_g, the PPO-*b*-PS copolymer is cheaper (in terms of having a lower PPO content) and easier to process (higher PS content) than is the PPO/PS blend. Here, we must emphasize that the pure PPO employed in this study has a lower glass transition temperature (163 °C; $M_w = 4000$) than that used in a previous study [33] (210 °C; $M_w = 11{,}000$) because of their different molecular weights, as has been discussed widely [49]. The lower-molecular-weight PPO is more easily converted to its PPO-Br macroinitiator by esterification of is high-weight PPO. The related results for high-molecular-weight PPO-*b*-PS copolymers will be reported later.

As also indicated in Fig. 7, the T_g breadth displays a positive deviation in PPO/PS blends. In general, a miscible polymer blend generally provides a broader DSC transition. In contrast, the PPO-*b*-PS copolymer exhibits a narrower T_g breadth than that of the PPO/PS blend, which implies that the block copolymer has better homogeneity at the molecular scale than does the polymer blend. Dynamic mechanical analysis (DMA) allows the molecular relaxation behavior of small chain segments to be detected and, thus, the phase heterogeneity can be detected on smaller scales than they can be by DSC. We performed DMA measurements to further investigate the miscibility of the PPO-*b*-PS copolymers. The apparently contradictory result between DSC and DMA in terms of T_g may be understood by considering the different experimental probe sizes. DMA is capable of identifying compositional heterogeneity at the ca. 5-nm scale, whereas DSC is sensitive only to heterogeneity on a scale >20 nm; heterogeneities smaller than this will be averaged out by this larger probe size [50]. A single value of T_g is observed in the DSC analysis of the PPO/PS blends, but the T_g breadth is broad. Fig. 8 displays a plot of tan δ of the PPO-*b*-PS copolymer (43PS) as a function of temperature. Clearly, only one sharp tan δ peak is located at ca. 160 °C, between the values observed for pure PS (120 °C) and pure PPO (180 °C), which indicates that the PPO-*b*-PS copolymer is miscible on the molecular scale (<5 nm), which is similar PPO/PS blend system [51].

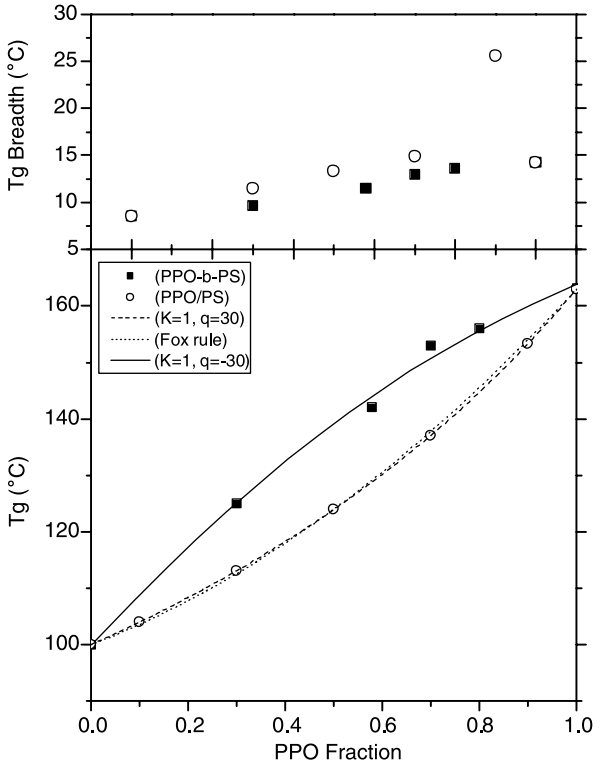

Fig. 7. Plots of the value and breadth of T_g versus the PPO content of PPO/PS blends and PPO-*b*-PS copolymers.

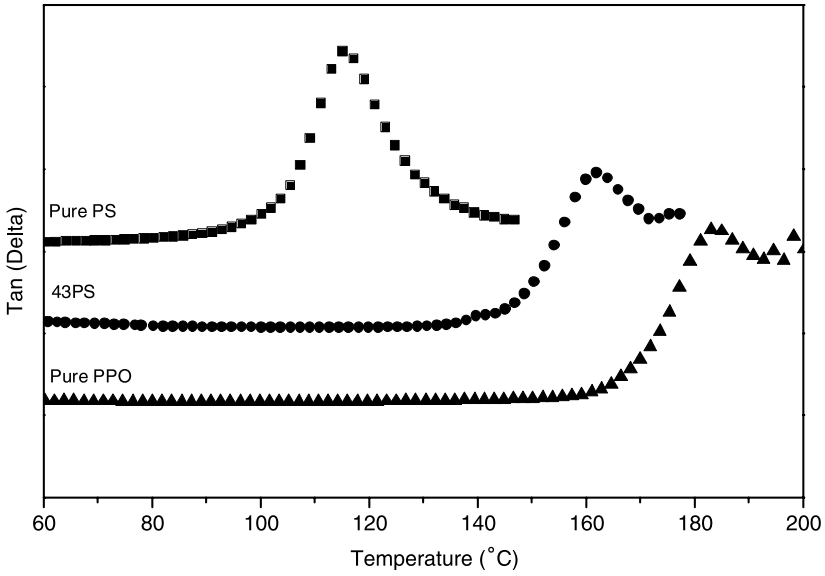

Fig. 8. Values of tan δ of pure PPO, pure PS, and 43PS copolymer plotted as a function of temperature.

3.3. Solid state NMR spectra of PPO-b-PS copolymers

Evidence for the specific interactions that exist in polymer blends and copolymers can be determined from changes in chemical shifts or line shapes in solid state NMR spectra. Moreover, the molecular mobility of a polymer blend or a copolymer can be estimated from the proton spin–lattice relaxation times in the rotating frame $\left(T_{1\rho}^{\mathrm{H}}\right)$, measured by solid state NMR spectroscopy. Fig. 9 presents the ^{13}C CP/MAS spectra of pure PPO, pure PS, various PPO/PS blends, and their PPO-*b*-PS copolymers, with peak assignments indicated in Scheme 2. The chemical shift of solid state NMR is different from the solution NMR since the conformation of PPO has the dihedral angles [52]. Table 3 summarizes the values of the chemical shifts observed in the ^{13}C CP/MAS NMR spectra of PPO/PS blends and PPO-*b*-PS copolymers. Compared with the ^{13}C CP/MAS NMR spectra of the pure PPO, the spectra of the PPO/PS blends and PPO-*b*-PS copolymers display significant changes, especially for the resonances of the carbon atoms that are involved in intermolecular interactions. Clearly, the signal of the methyl group of PPO shifts downfield upon increasing the PS content in both the blend and copolymer systems. This result is consistent with those

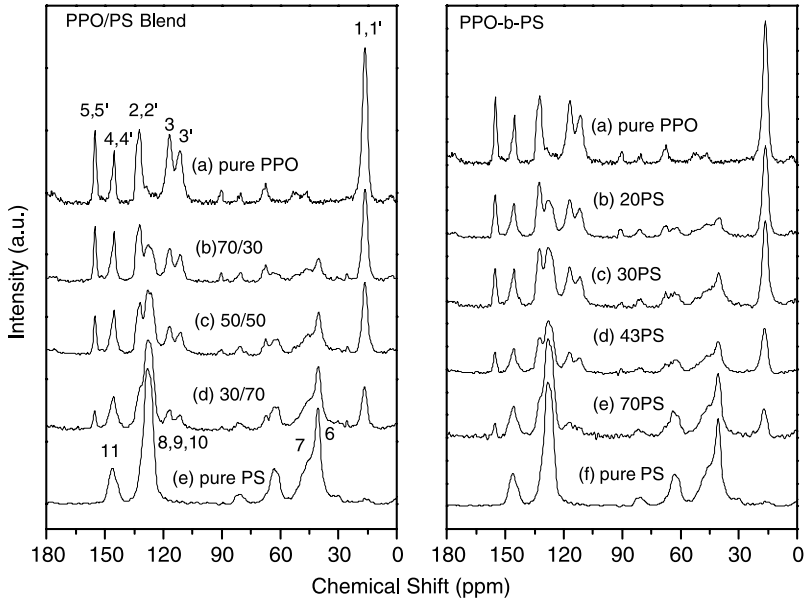

Fig. 9. ^{13}C CPMAS spectra recorded at room temperature for (a) PPO/PS blends and (b) PPO-*b*-PS copolymers.

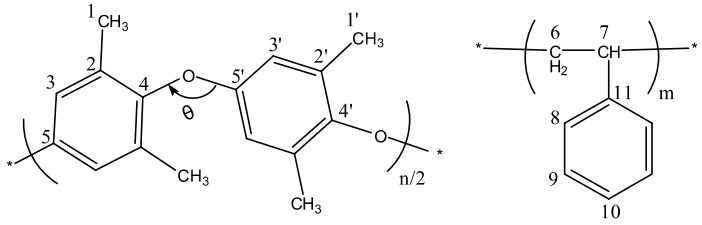

Scheme 2. Chemical structures of PPO and PS and their atom schemes in solid-state ^{13}C NMR [52].

of previous studies that have suggested that the specific interactions between PPO and PS units exist between the methyl groups of PPO and the phenyl rings of PS. Interestingly, Fig. 10 indicates that the chemical shifts of the methyl groups in the PPO-*b*-PS copolymer are greater than those of the corresponding PPO/PS blend, which suggests that the specific interactions are stronger within the PPO-*b*-PS copolymer than they are in the corresponding PPO/PS blend. This result is also consistent with the observed differences in the glass transition temperatures between the PPO-*b*-PS copolymer and PPO/PS blend.

3.4. Proton spin–lattice relaxation time in the rotating frame analyses

To better understand the differences between the glass transition temperature of the PPO-*b*-PS copolymers and the PPO/PS blends, we determined the molecular mobility of these systems based on their values of spin–lattice relaxation times in the rotating frame $\left(T_{1\rho}^{H}\right)$, which we obtained from solid state NMR spectra. The values of $T_{1\rho}^{H}$ allow the molecular mobility and homogeneity of the PPO-*b*-PS copolymer and PPO/PS blends to be measured on the molecular scale. To determine the values of $T_{1\rho}^{H}$, we monitored the low-field resonance at 154 ppm of the aromatic quarternary carbon atom of PPO and that of the backbone carbon atom of PS at 40 ppm and treated the results according to first-order kinetics. The $T_{1\rho}^{H}$ relaxation behavior of each blend and block copolymer is presented in Table 4 (PPO, 154 ppm; PS, 40 ppm), which reveals that both the PPO-*b*-PS copolymers and the PPO/PS blends exhibit only a single relaxation throughout all their compositions. This finding indicates that good miscibility and dynamic homogeneity exists in all of the copolymers

Table 3
Chemical shifts (ppm) observed in the ^{13}C CP/MAS/DD NMR spectra of PPO and PS units in their block copolymers and polymer blends

PPO/PS blend	PPO					
	C-1	C-2	C-3	C-4	C-5	C-6
Pure PPO	16.5	111.5	116.8	132.4	145.2	155.1
70/30	16.6	111.6	116.8	132.2	145.3	155.2
50/50	16.7	111.4	116.9	132.0	145.3	155.2
30/70	16.8	111.5	116.7	131.7	145.7	155.2
	PS					
	C-7	C-8	C-9, C-10 and C-11	C-12		
70/30	40.6	–	128.0	145.3		
50/50	40.4	–	128.1	145.3		
30/70	40.5	–	128.1	145.7		
Pure PS	40.7	–	128.2	146.1		
PPO-*b*-PS copolymer	PPO					
	C-1	C-2′	C-2	C-3	C-4	C-5
20PS	16.6	112.0	117.0	132.7	145.6	155.3
30PS	16.7	111.8	117.1	132.5	145.5	155.3
43PS	16.9	111.8	117.2	132.3	145.6	155.4
70PS	17.4	112.4	116.7	132.5	145.7	155.4
	PS					
	C-6	C-7	C-8, C-9 and C-10	C-11		
20PS	40.2	–	127.8	145.6		
30PS	40.5	–	128.1	145.5		
43PS	40.8	–	128.0	145.6		
70PS	40.8	–	128.1	145.7		

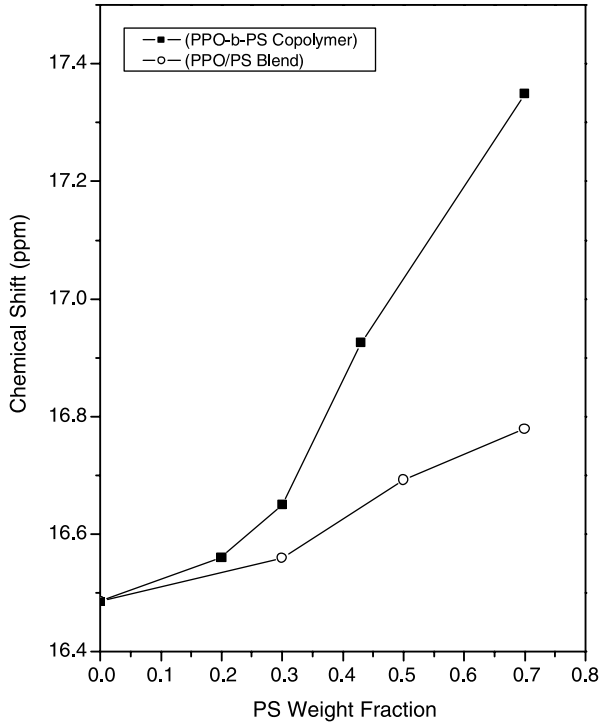

Fig. 10. The chemical shift of the methyl group of PPO as a function of the PS content in PPO/PS blends and PPO-*b*-PS copolymers.

and blends, which is consistent with the results of the DMA analysis. The single value of $T_{1\rho}^{H}$ obtained for each PPO-*b*-PS copolymer in all its compositions is higher than that for each corresponding PPO/PS blend. This observation suggests that retardation of the PPO-*b*-PS copolymers' mobility is relatively greater than that of the blend, which reflects the more-rigid character of the PPO-*b*-PS copolymer. Therefore, the glass transition temperatures of the

Table 4
Relaxation parameters for PPO/PS blends and PPO-*b*-PS copolymers

PPO/PS blends	$T_{1\rho}$(H) (μs)	
	At 40 ppm	At 154 ppm
Pure PPO	–	22.83
70/30	10.74	14.58
50/50	8.77	17.79
30/70	6.33	9.34
Pure PS	4.92	
PPO-*b*-PS	$T_{1\rho}$(H) (μs)	
28 PS	17.86	12.94
30 PS	14.74	15.61
43 PS	8.90	29.49
70 PS	7.53	20.35

PPO-*b*-PS copolymers are higher than their corresponding PPO/PS blends, which is consistent with the values of $T_{1\rho}^{H}$ determined by these solid state NMR analyses.

3.5. Two-dimensional FTIR analyses of PPO-b-PS copolymers

PPO/PS blends have been studied for many years and are classified as miscible blends, but the mechanism by which the chains interact has remained a point of contention. Many reports [15,16,18,19] have pointed out that the methyl groups of PPO take part in specific interactions with the aromatic groups of PS through the formation of π-cation complexes. Fig. 11 presents routine FTIR spectra of the PPO/PS blends and PPO-*b*-PS copolymers recorded at different compositions, and Table 5 lists detailed peak assignments of the PPO and PS segments. Fig. 12 displays synchronous 2D correlation maps of the PPO/PS blend in the range from 3200 to 2500 cm^{-1}; strong auto and cross

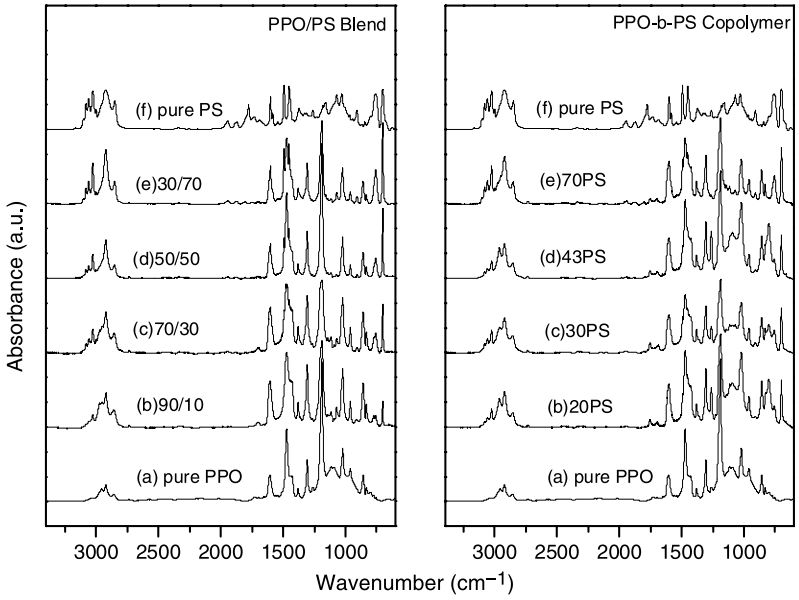

Fig. 11. One-dimensional FTIR spectra of (a) PPO/PS blends and (b) PPO-*b*-PS copolymers.

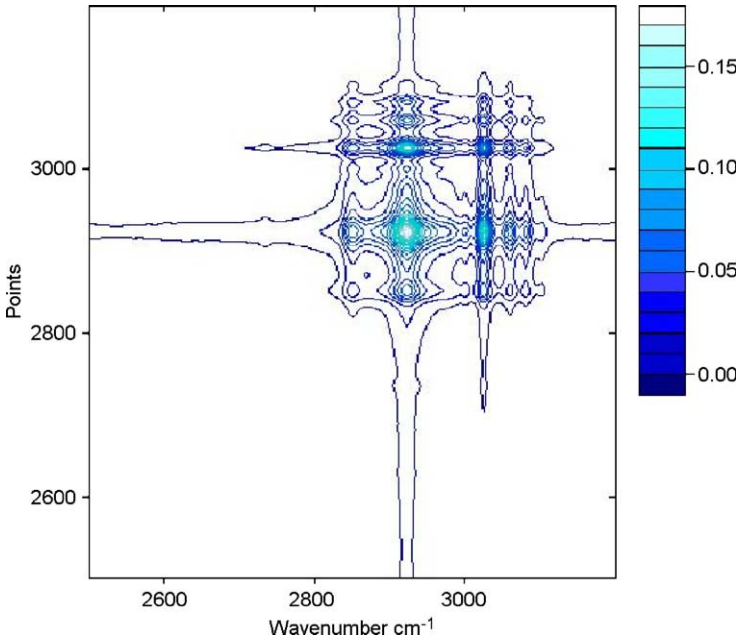

Fig. 12. Synchronous 2D correlation maps of PPO/PS blends.

peaks appear at wavenumbers $>3000\ cm^{-1}$. Fig. 12(a) presents the synchronous 2D correlation maps of the PPO-*b*-PS copolymer in the range from 3200 to 2500 cm^{-1}. In this spectral range, the bands for PS appear at 3002–3100 cm^{-1} (due to C–H stretching vibrations of the aromatic rings), at 2924 cm^{-1} (C–H asymmetric stretching vibrations), and at 2850 cm^{-1} (C–H symmetric stretching vibrations); those for PPO appear at 3002–3102 cm^{-1} (C–H stretching vibrations of the aromatic rings), 2925 cm^{-1} (C–H asymmetric stretching vibrations), and 2856 cm^{-1} (C–H symmetric stretching vibrations). In Fig. 13(a), many positive auto peaks and cross peaks appear at wavenumbers $<3000\ cm^{-1}$ as a result of contributions from the same chains, but no auto or cross peaks appear at wavenumbers $>3000\ cm^{-1}$, which indicates that the aromatic rings of PS and PPO have less rotational freedom relative to those same units in PPO/PS blends.

Fig. 13(b) displays the asynchronous 2D correlation map of the PPO-*b*-PS copolymer's spectra in the range from 3200 to 2500 cm^{-1}; we observe cross peaks having the opposite order of intensity. As mentioned in the Section 2, the asynchronous map is used to separate the bands of PPO from the spectra of PS in the blends or copolymers. Let us consider the reduced cross-correlation function, $X(\tau)$, defined by Noda [43]:

$$X(\tau) = \Phi(\nu_1, \nu_2)\cos(\omega\tau) + \Psi(\nu_1, \nu_2)\sin(\omega\tau) \quad (2)$$

In Eq. (2), the terms, $\Phi(\nu_1, \nu_2)$ and $\Psi(\nu_1, \nu_2)$ are regarded as the real and imaginary parts of the function and are referenced as the cross peak intensities in the asynchronous and synchronous correlation maps. The term ω is the external perturbation angular frequency. In the case where $\omega = 180$, $\cos(\omega t)$ equals zero and $\sin(\omega t)$ equals -1.0 and, therefore, we would obtain the weakest cross-peak intensity in the synchronous correlation maps. From a molecular level point of view, all of the aromatic rings would exist in vertical direction against that of the IR radiation. In another words, the PS segments exist in a regular rearrangement in the copolymers. As indicated in Fig. 7, the value of T_g displays a maximum for PPO-*b*-PS copolymers. This phenomenon, i.e. the higher value of T_g for the PPO-*b*-PS copolymers than for the PPO/PS blends, probably is caused by the regular rearrangement as the content of PS increases in the copolymers. Because the regular rearrangement is not

Table 5
Frequencies and assignments of the FTIR bands of pure PS and pure PPO

PS	PPO	Assignments
3002–3103	3002–3103	C–H aromatic stretching
	2925	C–H asymmetrical stretching
2924		C–H asymmetrical stretching
	2856	C–H symmetrical stretching
2850		C–H symmetrical stretching
	1610	C–C stretching frequency of ring in plane
1601		C–C stretching frequency of ring in plane
1583		C–H stretching vibration of ring in plane
1493		C–C stretching frequency of ring in plane
	1472	C–C aromatic stretching
1452		C–H deformation of CH_2
	1190	Asymmetric C–O–C stretching
1069		C–H bending vibration of ring in plane
	1030	C–H rocking vibration
1028		C–H bending vibration of ring in plane
	1020	C–H rocking vibration
	856	C–H bending
756		C–H out of plane bending vibration of ring
698		C–H out of plane bending vibration of ring

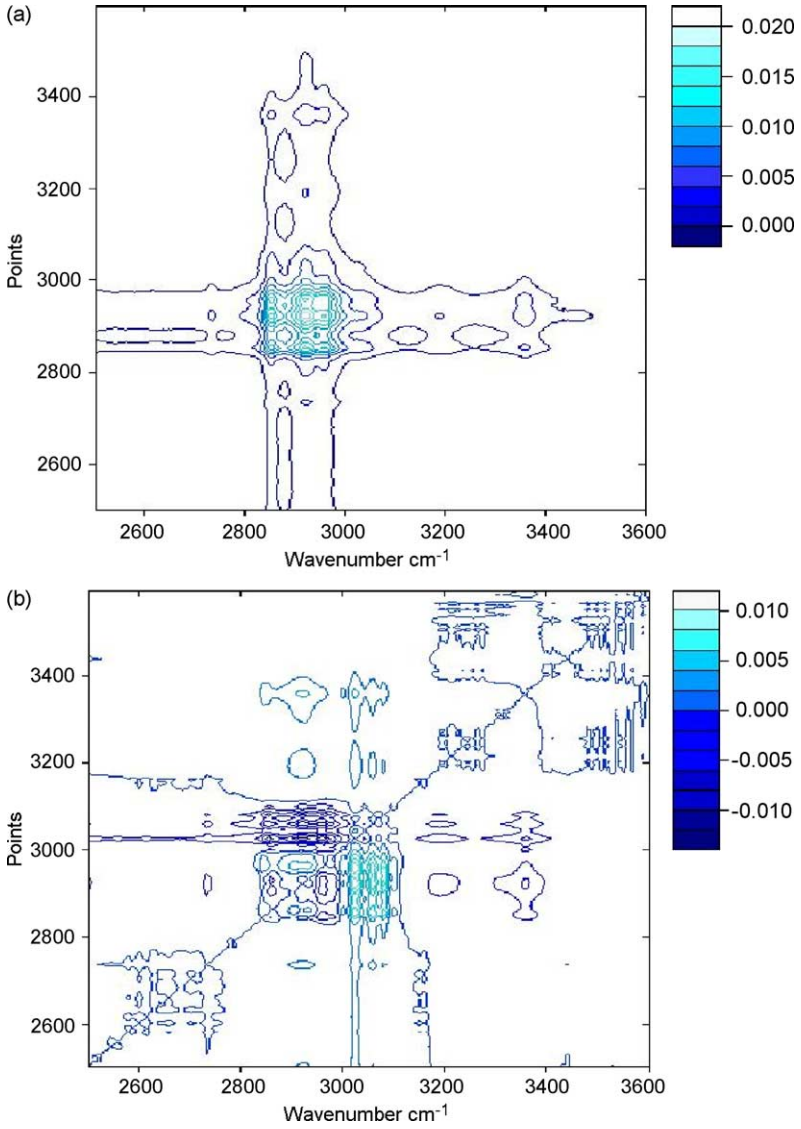

Fig. 13. Two dimensional correlation maps of the PPO-*b*-PS copolymer; (a) synchronous, (b) asynchronous.

so clearly formed in PPO/PS blends, the values of T_g in these cases exist as a linear combination of those of the two original components.

4. Conclusions

All of the thermal and spectroscopic methods of characterization we have employed in this study provide positive evidence that we have successfully synthesized block copolymers of PPO with PS. From DSC analyses, we observed higher glass transition temperatures for PPO-*b*-PS copolymers relative to their corresponding PPO/PS blends as a result of stronger specific interactions existing in the PPO-*b*-PS copolymer system. FTIR and solid state NMR spectroscopic analyses provided evidence that the specific interaction in the PPO-*b*-PS copolymer arises from the methyl group of PPO interacting with the aromatic rings of PS, similar to that observed for the PPO/PS blend system. We believe that this study provides an alternative novel approach to the creation of higher-T_g materials through the copolymerization of PPO and PS and that this method has the potential economically to replace classical miscible PPO/PS blend systems.

Acknowledgements

The authors would like to thank the National Science Council, Taiwan, Republic of China for financially supporting this research under Contract Nos. NSC-93-2216-E-009-018.

References

[1] Scultz AR, Beach DM. Macromolecules 1974;7:902.
[2] Prest WM, Porter RS. J Polym Sci, A-2 1972;10:1639.
[3] deAraujo MA, Stadler R, Cantow HJ. Polymer 1988;29:2235.
[4] Kuo SW, Chang FC. Macromolecules 2001;34:5224.
[5] Kuo SW, Xu H, Huang CF, Chang FC. J Polym Sci, Polym Phys Ed 2002;40:2313.
[6] Kuo SW, Chang FC. Polymer 2003;44:3021.
[7] Webster OW. Science 1994;251:887.
[8] Fréchet JMJ. Science 1994;263:1710.
[9] Reiss G, Hurtrez G, Bahadur P. Block copolymers. In: Korschwitz JI, editor. Encyclopedia of polymer science and engineering. New York: Wiley; 1985.
[10] Thomas EL, Anderson DM, Henkee CS, Hoffman D. Nature 1988; 334:598.
[11] Bates FS, Fredrickson GH. Annu Rev Phys Chem 1990;41:525.
[12] Bates FS. Science 1991;251:898.
[13] Schue F. In: Allen G, Bevirington JC, editors. Synthesis of block copolymers by transformation. Reactions in comprehensive polymer science, vol. 6. Oxford, UK: Pergamon Press; 1989 [chapter 10].
[14] Kennedy JP, Jacob S. Acc Chem Res 1998;31:835.
[15] Matyjaxzewski K, editor. Cationic polymerizations: Mechanisms, synthesis and applications. New York: Marcel Dekker; 1996.
[16] Szwarc M. Living polymers and election transfer processes. New York: Interscience; 1968.
[17] Hsieh HL, Quirk RP. Anionic polymerization: Principles and practical applications. New York: Marcel Dekker; 1996.
[18] Kato M, Kamigaito M, Sawamoto M, Higashimura T. Macromolecules 1995;28:1721.
[19] Patten TE, Xia J, Abernathy T, Matyjaszewski K. Science 1996;272: 866.
[20] Shipp DA, Wang JL, Matyjaszewski K. Macromolecules 1998;31: 8005.
[21] Muhlebach A, Gaynor SG, Matyjaszewski K. Macromolecules 1998; 31:6046.
[22] Angot S, Murthy KS, Taton D, Gnanou Y. Macromolecules 1998;31: 7218.
[23] Ueda J, Kamigaito M, Sawamoto M. Macromolecules 1998;31:6762.
[24] Wang JS, Matyjaszewski K. J Am Chem Soc 1995;117:5614.
[25] Wang JS, Matyjaszewski K. Macromolecules 1995;28:7901.
[26] Kalo M, Kamigaito M, Sawamoto M, Higashimura T. Macromolecules 1995;28:1721.
[27] Percec V, Barbooiu B. Macromolecules 1995;28:7970.
[28] Haddleton DM, Jasieczek CB, Hannon MJ, Shooter AJ. Macromolecules 1997;30:2190.
[29] Granel C, Dubois P, Jerome R, Teyssie P. Macromolecules 1996;29: 8579.
[30] Agari Y, Shimada M, Ueda A. Polymer 1997;38:2649.
[31] Robertson CG, Wilkes GL. Polymer 2000;41:9191.
[32] Li S, Rice DM, Karasz FE. Macromolecules 1994;27:2211.
[33] Cowie JMG, Harris S, Gomez-Ribelles JL, Meseguer JM, Romero F, Torregrosa CT. Macromolecules 1999;32:4430.
[34] Kawabata K, Fukuda T, Tsujii Y, Miyamoto T. Macromolecules 1993;26:3980.
[35] Coleman MM, Graf JF, Painter PC. Specific interactions and the miscibility of polymer blends. Lancaster, PA: Technomic Publishing; 1991.
[36] Hill DJT, Whittaker AK, Wong KW. Macromolecules 1999;32:5285.
[37] Kim JH, Min BR, Kim CK, Won J, Kang YS. J Phys Chem B 2002; 106:2786.
[38] Kuo SW, Chang FC. Macromolecules 2001;34:4089.
[39] Wang P, Jones AA, Inglefield PT, White DM, Bendler JT. New Polym Mater 1990;3:221.
[40] Djordjevic MB, Porter RS. Polym Eng Sci 1983;23:650.
[41] Goh SH, Lee SY, Zhou X, Tan KL. Macromolecules 1999;32:942.
[42] VanderHart DL. Macromolecules 1994;27:2837.
[43] Noda I. J Am Chem Soc 1989;111:8116.
[44] Nakashima K, Ren Y, Nishioka T, Tsubahara N, Noda I, Ozaki Y. Macromolecules 1999;32:6307.
[45] Huang H, Malkov S, Coleman MM, Painter PC. Macromolecules 2003;36:8156.
[46] Ma JC, Douberty DA. Chem Rev 1997;97:1303.
[47] Nishio M, Umezawa Y, Hirota M, Takeuchi Y. Tetrahedron 1995;51: 8665.
[48] Kwei TK. J Polym Sci, Polym Lett Ed 1984;22:307.
[49] O'Driscoll K, Sanayei RA. Macromolecules 1991;24:4479.
[50] Zhang S, Painter PC, Runt J. Macromolecules 2002;35:9403.
[51] Shultz AR, Beach BM. Macromolecules 1974;7:902.
[52] Bielecki A, Burum DP, Rice DM, Karasz FE. Macromolecules 1991; 24:4820.